JOURNAL OF PROPULSION AND POWER
Vol. 9, No. 4, July–Aug. 1993

Prediction of Turbulent Coaxial Streams of Constant and Variable Density

Richard W. Johnson*
EG&G Idaho, Inc., Idaho Falls, Idaho 83415

The present study investigates the accuracy of well-known turbulence models in simulating the mean velocity, turbulence, and concentration fields for the cases of constant and variable density, turbulent, low Mach number, isothermal, confined coaxial streams of different bulk mean velocities, or axisymmetric mixing layers. The standard $k \sim \varepsilon$ eddy viscosity model and an anisotropic thin shear algebraic stress model (ASM) are employed for the constant density case. Results for the $k \sim \varepsilon$ model are determined to be qualitatively satisfactory and superior to those for the thin shear ASM, though both show excessive radial diffusion of axial momentum. Based on these conclusions, the $k \sim \varepsilon$ model, extended for variable density, is used for numerical simulations of a similar flow where the inner stream gas has a density four times that of the outer stream gas. Simulations for the velocity using the $k \sim \varepsilon$ model are again found to be qualitatively accurate. Predictions for the concentration field, however, are in good agreement with the data. The flow fields studied are idealizations of a particular configuration once proposed for a gas core reactor (GCR) nuclear propulsion engine. Nuclear propulsion for space travel, once considered in the 1960s and early 1970s, is being reconsidered, especially for manned interplanetary travel.

Introduction

SINCE the goal of sending a manned mission to Mars was announced in 1989, interest in reconsidering the advantages of nuclear propulsion has increased greatly. A primary advantage of nuclear propulsion, for example, is the significantly reduced time required to make the round trip, minimizing the exposure of the travelers to cosmic radiation. Nuclear propulsion was once considered for use with space vehicles in the 1960s and early 1970s. One of the high-risk, high-potential propulsion concepts for space travel investigated then was the gas core reactor (GCR) nuclear propulsion engine. Operating at temperatures well above the vaporization temperature of uranium, the gas core reactor was to combine the dual attractions of theoretically high specific impulse and high thrust levels.

One of the configurations investigated in earlier times for the implementation of the gas core engine was the open cycle coaxial flow design, wherein the light hydrogen propellant would flow at a high rate around an inner core of slow moving, fissioning uranium vapor. The heavy uranium core would heat the hydrogen through convection and radiation heat transport. A number of experimental investigations were pursued during the 1960s and 1970s to determine and investigate the critical operating parameters of the coaxial gas core configuration. Two of the critical aspects of the design concept are the hydrodynamic and nuclear kinetic stabilities. The first issue relates to the question of being able to confine the gaseous fuel, minimizing its loss, while the second is concerned with being able to maintain a stable or at least controllable nuclear reaction.

One of the early experiments,[1] undertaken to investigate turbulent mixing of coaxial streams, examined the mixing of a slow inner stream with a faster outer stream surrounding it. Data were taken for various ratios of mean outer free-stream velocity to mean inner bulk velocity and for homogeneous and heterogeneous combinations of fluids. Because the boundary layer of the outer stream had time to transition to turbulence and because some of the inner streams were also turbulent, the coaxial flow can be described as an axisymmetric turbulent mixing layer.

The objectives of the present study are 1) to numerically simulate one of the homogeneous turbulent axisymmetric mixing layer flows of Zawacki and Weinstein[1] using two turbulence models to determine the suitability of each for this flow, and 2) to apply either of the two models that behaves satisfactorily for the homogeneous case to a similar heterogeneous case. The two turbulence models are the standard $k \sim \varepsilon$ model and an anisotropic thin shear algebraic stress model (ASM). Figure 1 provides a schematic diagram of the flow geometry and conditions for the constant and variable density axisymmetric mixing layers.

An early numerical simulation of the data of Zawacki and Weinstein[1] for the same case investigated here was reported by Zelazny et al.[2] They derived a highly empirical, eddy viscosity model for the turbulent shear stress based on data for axisymmetric jets, wakes, and coflowing streams. They initiated their calculations downstream of the initial point of

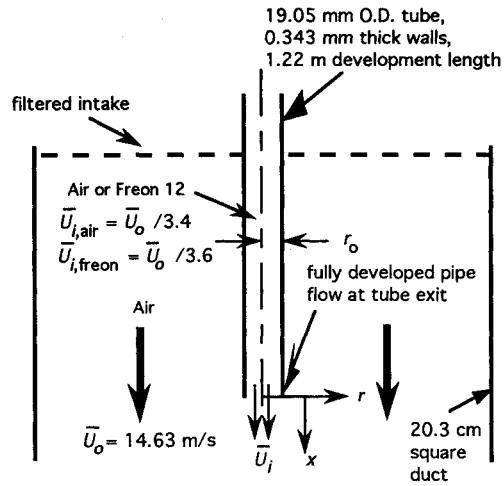

Fig. 1 Schematic diagram of the geometry and boundary conditions for the coaxial jets.

Received Dec. 5, 1991; revision received Dec. 7, 1992; accepted for publication Jan. 25, 1993.

*Senior Engineering Specialist, Idaho National Engineering Laboratory.

mixing where the data are complete enough to apply their model. Their calculations for two additional downstream stations show quite good agreement. However, because the turbulence model is so highly empirical, it would seem imprudent to apply the model to flows much different than the flow on which it is based.

Several experimental and/or numerical studies have been made in the past several years documenting coaxial jet flows. Ribeiro and Whitelaw[3] report experimental data of coaxial jets having identical maximum velocities issuing from a pipe and concentric annulus into unconfined stagnant surroundings. They discuss the importance of turbulent diffusion in the flow development, indicating that it balances the dissipation of turbulent kinetic energy. Hence, the developing flow is nonequilibrium in terms of the turbulent kinetic energy. (An equilibrium flow is where production of turbulent kinetic energy balances dissipation.) They also point out that a full second-moment turbulence closure would be required to get all of the turbulence quantities correct, though a simpler model could be used for engineering calculations where qualitative features are of primary interest. Habib and Whitelaw[4] report experiments and simulations of confined coaxial jets where the confinement includes an expansion at the initial plane of mixing (as in a jet engine combustor can). They compare data using a laser-Doppler anemometer (LDA) with earlier data taken in the same apparatus using a hot-wire. They found discrepancies of up to 10% in the mean data and up to 17% in the rms data. They further decided that the mean data are too high vs reality, while the rms data are too low, especially where rms data are greater than 30% of the magnitude of the mean data. Their calculations, employing the $k \sim \varepsilon$ turbulence model, show reasonable agreement downstream of the primary mixing region, but are inaccurate in the upstream area. The calculations for their nonswirling case are more accurate than those for the swirling case. In a later paper, Ribeiro and Whitelaw[5] report data for coaxial jet flows having different maximum velocity ratios. They again emphasize the importance of turbulent diffusion. They further recommend the use of a turbulence model like that of Bradshaw et al.[6] which employs a diffusion parameter based on a velocity characteristic of the large-scale motion of the turbulent eddies present in the flow. Such a diffusion term is added to try and capture the diffusion due to large-scale eddies which significantly contribute to the mixing process.

Wagner et al.[7] report numerical simulations of the flowfield of two confined coaxial jets with a sudden expansion (jet engine combustor). The sudden expansion generates a region of recirculating flow outside the jet mixing region. They employ a two-equation turbulence model with a large-scale diffusion term and compare results with data[8] and with earlier calculations using a low Reynolds number $k \sim \varepsilon$ model.[9] They find that the model employing the extra large-scale diffusion term provides for more diffusion, yielding more accurate results than does the other model. They attribute this to the ability of the model to handle countergradient turbulent diffusion which is a result of the large-scale motions. The nature of the countergradient diffusion is the subject of a related paper by Brondum and Bennett[10] which characterizes the regions of the flow of Ref. 8 where mass transport in the axial direction is against the gradient of species concentration. Brondum and Bennett[10] are able to show that the region of countergradient mass transport generally maps onto the region where large-scale eddies account for much of the mass transport. Of course, the contributions of radial diffusion to the overall transport of axial momentum and species are significantly larger than those of the axial components.

Sturgess and Syed[11] numerically investigate the flowfield of widely spaced, confined coaxial jets, as are found in a jet diffusion-flame combustor. They employ the $k \sim \varepsilon$ model and report excellent qualitative results; however, they also report shortcomings with the turbulence model in regions exhibiting streamline curvature. In their discussion of the suitability of the turbulence model, however, Sturgess and Syed seem to indicate that the $k \sim \varepsilon$ model assumes equilibrium between production and dissipation of turbulent energy. This is only true in the assignment of the viscosity coefficient (C_μ) to a constant value. The standard $k \sim \varepsilon$ model accounts for the production, dissipation, convection, and (gradient) diffusion of turbulent energy.

A number of studies have been performed for the related flows of planar mixing layers and wakes. The level of turbulence models employed for simulating such flows ranges from simple mixing length models to sophisticated second-moment closures. The study of Launder et al.[12] compares the results for a mixing length model and one and two equation turbulence models for the simulation of a plane mixing layer. Predictions for the transverse distributions of the mean streamwise velocity and the turbulent shear stresses are compared with experiments at two streamwise stations. The results for the $k \sim \varepsilon$ model are found to be very good for the mean velocity, while the other models show excessive diffusion. However, the $k \sim \varepsilon$ results for the shear stress, found to be good for the earlier streamwise station, are off by more than 100% for the station farther downstream! It is concluded by Launder et al.[12] that the shear stress data are suspect.

The conference report by Rodi[13] describes a large number of turbulence modeling studies presented at the EUROMECH Colloquium 180 held in Karlsruhe, Germany, July 4–6, 1984. Summaries of studies relating to mixing layers and wakes by Radespiel, Schiestel, and Jones are presented therein. Radespiel employs a three-equation $k \sim \varepsilon \sim \gamma$ turbulence model to simulate a plane mixing layer; γ, the intermittency factor, is modeled with a transport equation similar to those for k and ε. Schiestel uses a multiscale ASM where the energy spectrum is divided into two ranges with equations for turbulence quantities provided for each range. He gives results for a plane wake. Jones reports computations for a plane mixing layer with a full second-moment closure. In each of these three cases, the spreading rates for the mixing layer or wake are underpredicted, although improvements over results for the standard $k \sim \varepsilon$ model are reported for the first two studies.

Gross similarities exist between the flow studied here and the wake flow behind a bluff body. A successful study of such a flow is given by Biringen[14] who reports simulations for an axisymmetric wake flow for a body of revolution using a three-equation model of turbulence. The three turbulence parameters for which transport equations are solved are the turbulent kinetic energy and shear stress, and an integral length scale. Results for one axial station are presented for the wake flow. Agreement for the radial distribution of the mean streamwise velocity is shown to be quite good, although the distributions for turbulent kinetic energy and shear stress are less satisfactory.

Further examples of second-moment closures applied to mixing layers and wakes are provided by Launder et al.[15] and Lewellen et al.[16] Both report good results for mean velocities and Reynolds stresses, although complete agreement is not achieved. Nallasamy[17] reports $k \sim \varepsilon$ model predictions for the complex flow of confined coaxial turbulent jets issuing into an abrupt pipe expansion where there are recirculation zones in the corners and the central mixing region. He reports that the locations, sizes, and shapes of the recirculation zones along with axial and radial velocities and axial turbulence intensities are predicted fairly well, although the rate of redevelopment of the flow beyond reattachment is not.

It is further reported[13] that spreading rates for round jets are overpredicted, while those for planar wakes are underpredicted, using the same turbulence model. It therefore seems prudent to test models for axisymmetric geometry even if they have been found to work well for planar flows. The present study examines numerical simulations for constant and variable density coaxial streams (with thick boundary layers at the beginning of the mixing region).

The describing equations and closures for the cases of constant and variable density coflowing streams are detailed in the following two sections.

Describing Equations for Constant Density

Mean Fluid Flow Equations

The Reynolds-averaged continuity and Navier-Stokes equations for two dimensions are employed for the constant density, stationary, isothermal, axisymmetric problem of coflowing streams. We decompose the instantaneous velocity and pressure into simple ensemble mean and fluctuating components. Because the flows studied herein are stationary, the ensemble and time averages (over a suitably long time interval) are equivalent. The ensemble or time mean velocities are represented by $\bar{U}$ and $\bar{V}$ in the x and r directions, respectively. Corresponding fluctuating quantities are represented by u' and v'. w' is the circumferential fluctuation. The equations in cylindrical coordinates are

continuity

$$\frac{\partial \bar{U}}{\partial x} + \frac{\partial r\bar{V}}{r\partial r} = 0 \tag{1}$$

momentum

$$\frac{\partial \bar{U}\bar{U}}{\partial x} + \frac{\partial r\bar{V}\bar{U}}{r\partial r} = -\frac{1}{\rho}\frac{\partial \bar{\mathcal{P}}}{\partial x} + \frac{\partial}{\partial x}\left[2\nu\frac{\partial \bar{U}}{\partial x} - \overline{u'^2}\right] + \frac{\partial}{r\partial r}r\left[\nu\left(\frac{\partial \bar{U}}{\partial r} + \frac{\partial \bar{V}}{\partial x}\right) - \overline{u'v'}\right] \tag{2}$$

$$\frac{\partial \bar{U}\bar{V}}{\partial x} + \frac{\partial r\bar{V}\bar{V}}{r\partial r} = -\frac{1}{\rho}\frac{\partial \bar{\mathcal{P}}}{\partial r} + \frac{\partial}{\partial x}\left[\nu\left(\frac{\partial \bar{U}}{\partial r} + \frac{\partial \bar{V}}{\partial x}\right) - \overline{u'v'}\right] + \frac{\partial}{r\partial r}r\left[2\nu\frac{\partial \bar{V}}{\partial r} - \overline{v'^2}\right] + \frac{\overline{w'^2}}{r} - 2\nu\frac{\bar{V}}{r^2} \tag{3}$$

The quantities $\overline{u'^2}$, $\overline{v'^2}$, $\overline{w'^2}$, and $\overline{u'v'}$ are the kinematic Reynolds stresses. The thermodynamic pressure is $\mathcal{P}$ and the kinematic viscosity is represented by ν. The Reynolds stresses must be modeled in order to close the system. The two turbulence models employed for closure for the constant density case are given in the following section.

Turbulence Models

The first turbulence model used for the constant density case is the standard $k \sim \varepsilon$ eddy viscosity model.[18,19] The $k \sim \varepsilon$ model employs the following expressions for the kinematic Reynolds stresses:

$$-\overline{u'^2} = 2\nu_t\frac{\partial \bar{U}}{\partial x} - \frac{2}{3}k, \quad -\overline{v'^2} = 2\nu_t\frac{\partial \bar{V}}{\partial r} - \frac{2}{3}k$$

$$-\overline{w'^2} = 2\nu_t\frac{\bar{V}}{r} - \frac{2}{3}k, \quad -\overline{u'v'} = \nu_t\left(\frac{\partial \bar{U}}{\partial r} + \frac{\partial \bar{V}}{\partial x}\right) \tag{4}$$

The kinematic turbulent viscosity ν_t is modeled as $\nu_t = C_\mu k^2/\varepsilon$, where $k \equiv 0.5\,(\overline{u'^2} + \overline{v'^2} + \overline{w'^2})$ is the turbulent kinetic energy and ε its rate of dissipation. The turbulence quantities k and ε are determined from modeled transport equations given in cylindrical coordinates as

$$\frac{\partial \bar{U}k}{\partial x} + \frac{\partial r\bar{V}k}{r\partial r} = \frac{\partial}{\partial x}\left(\frac{\nu + \nu_t}{\sigma_k}\right)\frac{\partial k}{\partial x} + \frac{1}{r}\frac{\partial}{\partial r}r\left(\frac{\nu + \nu_t}{\sigma_k}\right)\frac{\partial k}{\partial r} + P - \varepsilon \tag{5}$$

$$\frac{\partial \bar{U}\varepsilon}{\partial x} + \frac{\partial r\bar{V}\varepsilon}{r\partial r} = \frac{\partial}{\partial x}\left(\frac{\nu + \nu_t}{\sigma_\varepsilon}\right)\frac{\partial \varepsilon}{\partial x} + \frac{1}{r}\frac{\partial}{\partial r}r\left(\frac{\nu + \nu_t}{\sigma_\varepsilon}\right)\frac{\partial \varepsilon}{\partial r} + C_{\varepsilon 1}\frac{\varepsilon}{k}P - C_{\varepsilon 2}\frac{\varepsilon^2}{k} \tag{6}$$

where the kinematic production of turbulent kinetic energy P in cylindrical coordinates is

$$P = \nu_t\left[2\left(\frac{\partial \bar{U}}{\partial x}\right)^2 + 2\left(\frac{\partial \bar{V}}{\partial r}\right)^2 + 2\left(\frac{\partial \bar{U}}{\partial r}\frac{\partial \bar{V}}{\partial x}\right) + \left(\frac{\partial \bar{U}}{\partial r}\right)^2 + \left(\frac{\partial \bar{V}}{\partial x}\right)^2 + 2\frac{\bar{V}^2}{r^2}\right] \tag{7}$$

The modeling coefficients are given the optimized values, $C_\mu = 0.09$, $\sigma_k = 1.0$, $\sigma_\varepsilon = 1.22$, $C_{\varepsilon 1} = 1.44$, and $C_{\varepsilon 2} = 1.92$.[19,20] The value employed for σ_ε is different than the widely used 1.3.[19] The present value is often used instead,[21] as it has a more theoretical base. The lower value is derived from the ε transport equation simplified for flow in the inertial sublayer near a flat boundary where convection is assumed zero, $P/\varepsilon \approx 1$, k is assumed constant, $\varepsilon = C_\mu^{0.75}k^{1.5}/(\kappa y)$ with the von Karman constant $\kappa = 0.419$,[20] giving $\sigma_\varepsilon = \kappa^2/[C_\mu^{0.5}(C_{\varepsilon 2} - C_{\varepsilon 1})] = 1.22$.

Inlet values for $\bar{U}$, k, ε, and ν_t were obtained from numerical simulations of pipe and annular flows. The wall treatment used for these precursory simulations was the standard wall function approach detailed in Launder and Spalding.[19] The inlet conditions for the annular part of the inlet plane were obtained by matching annular flow computations with the data point which lies in the annular boundary layer at $x/r_0 = 0$ given in Zawacki and Weinstein.[1] The inlet conditions for the pipe portion of the flow are fully developed turbulent pipe flow. For the far radial boundary condition, both free- and no-slip conditions are used as will be discussed later. The standard wall functions are used in the coflowing domain at the outer boundary for the no-slip case. The flow data are specified as having zero gradient at the outlet of the computational domain. The outlet boundary condition was validated by doubling the axial computational domain for one calculation and comparing results using the standard domain; the plotted results were indistinguishable.

The second turbulence model employed in the present study is a thin shear form of the ASM of Rodi.[22] In the thin shear version of the ASM, all mean velocity gradients are neglected except for the radial gradient of the mean streamwise velocity, which is much greater than any other for this problem. The model employed by the ASM for the Reynolds stresses is given as

$$\overline{u_i'u_j'} = \frac{k(1 - C_2)}{\varepsilon(C_1 - 1 + P/\varepsilon)}\left(P_{ij} - \frac{2}{3}\delta_{ij}P\right) + \frac{2}{3}\delta_{ij}k \tag{8}$$

P_{ij} and P are the production tensor for the Reynolds stresses and the production of k, respectively. For the present thin shear flow version of the ASM, P is given as

$$P = -\left[\overline{u'v'}\frac{\partial \bar{U}}{\partial r} + \overline{w'^2}\frac{\bar{V}}{r}\right] \tag{9}$$

The four components of the production tensor that are required for the ASM are approximated as

$$P_{12} = -\overline{v'^2}\frac{\partial \bar{U}}{\partial r}, \quad P_{11} = -2\overline{u'v'}\frac{\partial \bar{U}}{\partial r} \approx 2P$$

$$P_{22} = P_{33} = 0 \tag{10}$$

Employing these relations along with Eq. (8), the Reynolds stresses are modeled as

$$-\overline{u'v'} = \frac{2}{3}\frac{k^2}{\varepsilon}(1 - C_2)\frac{(C_1 - 1 + C_2P/\varepsilon)}{(C_1 - 1 + P/\varepsilon)^2}\frac{\partial \tilde{U}}{\partial r} \quad (11)$$

$$-\overline{v'^2} = -\overline{w'^2} = -\frac{2}{3}k\frac{(C_1 - 1 + C_2P/\varepsilon)}{(C_1 - 1 + P/\varepsilon)} \quad (12)$$

$$-\overline{u'^2} = -\frac{2}{3}k\frac{[C_1 - 1 + 1.5(2 - C_2)P/\varepsilon]}{(C_1 - 1 + P/\varepsilon)} \quad (13)$$

Transport equations are again required for k and ε. The transport equations used for the thin shear ASM for k and ε are

$$\frac{\partial \tilde{U}k}{\partial x} + \frac{\partial r\tilde{V}k}{r\partial r} = \frac{\partial}{\partial x}\left(\nu + C_{k1}\frac{k}{\varepsilon}\overline{u'^2}\right)\frac{\partial k}{\partial x} + \frac{\partial}{r\partial r}r\left(\nu + C_{k1}\frac{k}{\varepsilon}\overline{v'^2}\right)\frac{\partial k}{\partial r} + P - \varepsilon \quad (14)$$

$$\frac{\partial \tilde{U}\varepsilon}{\partial x} + \frac{\partial r\tilde{V}\varepsilon}{r\partial r} = \frac{\partial}{\partial x}\left(\nu + C_{\varepsilon}\frac{k}{\varepsilon}\overline{u'^2}\right)\frac{\partial \varepsilon}{\partial x} + \frac{\partial}{r\partial r}\left(\nu + C_{\varepsilon}\frac{k}{\varepsilon}\overline{v'^2}\right)\frac{\partial \varepsilon}{\partial r} + C_{\varepsilon 1}\frac{\varepsilon}{k}P - C_{\varepsilon 2}\frac{\varepsilon^2}{k} \quad (15)$$

where P is given by Eq. (9). The model coefficients for the ASM are $C_1 = 1.8$, $C_2 = 0.6$,[23] $C_{k1} = 0.22$,[24] $C_\mu = 0.09$, $C_{\varepsilon 1} = 1.44$, $C_{\varepsilon 2} = 1.92$,[12] and $C_\varepsilon = 0.17$.[25]

The inlet conditions used for the ASM computations are computed from precursory calculations similar to the $k \sim \varepsilon$ case, except that the ASM is used. The standard wall corrections for the ASM are employed for these calculations.[20] The same boundary conditions are used for the ASM simulations as for the $k \sim \varepsilon$ model predictions.

Describing Equations for Variable Density

Mean Fluid Flow Equations

For the variable density case, Favre or mass-weighted averaging is employed for the velocity. We can write

$$U = \tilde{U} + u'' \quad (16)$$

where

$$\tilde{U} \equiv (\overline{\rho U}/\bar{\rho}) \quad (17)$$

The flat overbar indicates simple time averaging as before. Note that the time average of u'' is not zero as are those for u', ρ', etc. Other quantities are subjected to simple time averaging ($\mathcal{P}$, ρ). The molecular viscosity is assumed to be constant and equal to that for air as the primary momentum and mass diffusion transports are turbulent. The two species present are assumed to be conserved according to the species continuity equation

species continuity

$$\frac{\partial}{\partial x}\bar{\rho}\tilde{U}\left(\frac{\bar{\rho}^s}{\bar{\rho}}\right) + \frac{\partial}{r\partial r}r\bar{\rho}\tilde{V}\left(\frac{\bar{\rho}^s}{\bar{\rho}}\right) = \frac{\partial}{\partial x}\bar{\rho}D\frac{\partial}{\partial x}\left(\frac{\bar{\rho}^s}{\bar{\rho}}\right) + \frac{\partial}{r\partial r}r\bar{\rho}D\frac{\partial}{\partial r}\left(\frac{\bar{\rho}^s}{\bar{\rho}}\right) \quad (18)$$

where the superscript s refers to species s and D is the turbulent diffusion coefficient. D is computed from the turbulent Schmidt number taken to be $Sc_t = \nu_t/D = 0.9$. The value 0.9 is that recommended by Launder[26] for the turbulent Prandtl number which is analogous to Sc_t. The overall mass and momentum conservation equations are given by

continuity

$$\frac{\partial \bar{\rho}\tilde{U}}{\partial x} + \frac{\partial r\bar{\rho}\tilde{V}}{r\partial r} = 0 \quad (19)$$

momentum

$$\frac{\partial \bar{\rho}\tilde{U}\tilde{U}}{\partial x} + \frac{\partial r\bar{\rho}\tilde{V}\tilde{U}}{r\partial r} = -\frac{\partial \bar{\mathcal{P}}}{\partial x} + \frac{\partial}{\partial x}\left[2\mu\frac{\partial \tilde{U}}{\partial x} - \overline{\rho u''^2} - \frac{2}{3}\mu\left(\frac{\partial \tilde{U}}{\partial x} - \frac{\partial r\tilde{V}}{r\partial r}\right)\right] + \frac{\partial}{r\partial r}r\left[\mu\left(\frac{\partial \tilde{U}}{\partial r} + \frac{\partial \tilde{V}}{\partial x}\right) - \overline{\rho u''v''}\right] \quad (20)$$

$$\frac{\partial \bar{\rho}\tilde{U}\tilde{V}}{\partial x} + \frac{\partial r\bar{\rho}\tilde{V}\tilde{U}}{r\partial r} = -\frac{\partial \bar{\mathcal{P}}}{\partial r} + \frac{\overline{\rho w''^2}}{r} + \frac{\partial}{\partial x}\left[\mu\left(\frac{\partial \tilde{U}}{\partial r} + \frac{\partial \tilde{V}}{\partial x}\right) - \overline{\rho u''v''}\right] + \frac{\partial}{r\partial r}r\left[2\mu\frac{\partial \tilde{V}}{\partial r} - \overline{\rho v''^2} - \frac{2}{3}\mu\left(\frac{\partial \tilde{U}}{\partial x} + \frac{\partial r\tilde{V}}{r\partial r}\right)\right] - 2\mu\frac{\tilde{V}}{r^2} + \frac{2}{3}\mu\left(\frac{\partial \tilde{U}}{\partial x} + \frac{\partial r\tilde{V}}{r\partial r}\right) \quad (21)$$

The ideal gas equation for multiple species is used to compute the overall density

$$\bar{\rho} = \left[\bar{\mathcal{P}}\Big/\sum_s\left(\frac{\bar{\rho}^s}{\bar{\rho}}\right)\frac{R\tilde{T}}{W_s}\right] \quad (22)$$

where T is the absolute temperature, R is the universal gas constant, and W_s is the molal mass for species s. The Reynolds stresses are the quantities $\rho u''^2$, $\rho v''^2$, $\rho w''^2$, and $\rho u''v''$ which are based on the fluctuating components of the mass-weighted velocity. The dynamic viscosity is represented by μ. The turbulence model used to model the Reynolds stresses for the variable density case is given in the following section.

Turbulence Model

The turbulence model used for the variable density case is the $k \sim \varepsilon$ model extended to variable density. We employ the following to model the Reynolds stresses:

$$\begin{aligned}
-\overline{\rho u''^2} &= \mu_t\left[2\frac{\partial \tilde{U}}{\partial x} - \frac{2}{3}\left(\frac{\partial \tilde{U}}{\partial x} + \frac{\partial r\tilde{V}}{r\partial r}\right)\right] - \frac{2}{3}\bar{\rho}k \\
-\overline{\rho v''^2} &= \mu_t\left[2\frac{\partial \tilde{V}}{\partial r} - \frac{2}{3}\left(\frac{\partial \tilde{U}}{\partial x} + \frac{\partial r\tilde{V}}{r\partial r}\right)\right] - \frac{2}{3}\bar{\rho}k \\
-\overline{\rho w''^2} &= \mu_t\left[2\frac{\tilde{V}}{r} - \frac{2}{3}\left(\frac{\partial \tilde{U}}{\partial x} + \frac{\partial r\tilde{V}}{r\partial r}\right)\right] - \frac{2}{3}\bar{\rho}k \\
-\overline{\rho u''v''} &= \mu_t\left(\frac{\partial \tilde{U}}{\partial r} + \frac{\partial \tilde{V}}{\partial x}\right)
\end{aligned} \quad (23)$$

Note that the mass-weighted mean velocity gradients are used in modeling the Reynolds stresses even though the unweighted mean strain rates appear in the momentum equations. This is simply a modeling decision.

The kinematic turbulent viscosity μ_t is modeled as $\mu_t = \bar{\rho} C_\mu k^2/\varepsilon$. Mass averaging is also applied to the turbulent kinetic energy:

$$k \equiv (\overline{\rho u_i'' u_i''}/\bar{\rho}) \tag{24}$$

The transport equations for k and ε, extended for variable density, are

$$\frac{\partial \bar{\rho}\tilde{U}k}{\partial x} + \frac{\partial r\bar{\rho}\tilde{V}k}{\partial r} = \frac{\partial}{\partial x}\left(\frac{\mu + \mu_t}{\sigma_k}\right)\frac{\partial k}{\partial x} + \frac{\partial}{r\partial r} r\left(\frac{\mu + \mu_t}{\sigma_k}\right)\frac{\partial k}{\partial r} + P - \bar{\rho}\varepsilon \tag{25}$$

$$\frac{\partial \bar{\rho}\tilde{U}\varepsilon}{\partial x} + \frac{\partial r\bar{\rho}\tilde{V}\varepsilon}{\partial r} = \frac{\partial}{\partial x}\left(\frac{\mu + \mu_t}{\sigma_\varepsilon}\right)\frac{\partial \varepsilon}{\partial x} + \frac{\partial}{r\partial r} r\left(\frac{\mu + \mu_t}{\sigma_\varepsilon}\right)\frac{\partial \varepsilon}{\partial r} + C_{\varepsilon 1}\frac{\varepsilon}{k}P - C_{\varepsilon 2}\bar{\rho}\frac{\varepsilon^2}{k} \tag{26}$$

where the production of k is now given by

$$P = \mu_t\left[2\left(\frac{\partial \tilde{U}}{\partial x}\right)^2 + 2\left(\frac{\partial \tilde{V}}{\partial r}\right)^2 + 2\left(\frac{\partial \tilde{U}}{\partial r}\frac{\partial \tilde{V}}{\partial x}\right) + \left(\frac{\partial \tilde{U}}{\partial r}\right)^2 + \left(\frac{\partial \tilde{V}}{\partial x}\right)^2 + 2\frac{\tilde{V}^2}{r^2} - \frac{2}{3}\left(\frac{\partial \tilde{U}}{\partial x} + \frac{\partial r\tilde{V}}{r\partial r}\right)^2\right] - \frac{2}{3}\bar{\rho}k\left(\frac{\partial \tilde{U}}{\partial x} + \frac{\partial r\tilde{V}}{r\partial r}\right) \tag{27}$$

In view of the fact that the present coflowing streams are far from walls, the contributions due to terms involving molecular viscosity and gradients of $\overline{u''}$ are neglected. Hence, the diffusion terms in the momentum equations are modeled to involve only the mass-weighted mean strain rates.

Computing Details

The describing equations are solved using a steady, implicit finite volume code based on the staggered mesh SIMPLE algorithm of Patankar and Spalding.[27] The code belongs to the TEACH family[28] of finite volume codes. The iterative procedure of SIMPLE is executed until totaled mass and momentum residuals are each less than $1.0 \times 10^{-5}\%$. The grid used for free-slip, constant density calculations is 60×52 cells, while that for the no-slip cases is 66×81. The same finer grid used for the constant density case is used for the variable density case. The cells expand in length in the axial direction and radially beyond the inner tube location toward the outer radius. The cross-sectional area of the cylindrical computational domain is configured to have the same perimetral length as the square-sectioned test section of the experimental apparatus of Zawacki and Weinstein.[1] The mesh is especially fine near the inner and outer walls of the inner tube. The HYBRID scheme (upwinding for cell Reynolds number $Re_\Delta > 2$, centered differencing for $Re_\Delta < 2$) is used in the calculations. Typical run time for a simulation is 250 s on the INEL CRAY XMP/216.

Validation computations were made to compare $k \sim \varepsilon$ results for the same constant density plane mixing layer computed by Launder et al.[12] Computed profiles of mean velocity and shear stress (not shown) were found to be very close to the calculations of Launder et al.[12]

Results and Discussion

Constant Density Case

Experimental data are provided by Zawacki and Weinstein[1] for several different ratios of outer to inner bulk mean velocities for the axisymmetric coaxial stream problem. While the same velocity is used for the outer stream in all cases, the bulk velocity of the inner stream is varied to obtain the different velocity ratios. Of these several experiments, only two involve inner streams that are fully turbulent: $\bar{U}_0/\bar{U}_i = 1.0$ and 3.4; we choose the latter for the present study. For this ratio, the Reynolds number of the inner stream is $Re = 2r_0\bar{U}_i/\nu \sim 5000$.

The experimental data for the radial variation of the mean streamwise velocity are given in Zawacki and Weinstein[1] for several axial stations along the axisymmetric mixing layer. Unfortunately, the inlet data are incomplete because only mean velocities are given. As mentioned earlier, the inlet data for the turbulence quantities are obtained from simulations made earlier for pipe and annular flows. Figure 2 presents results for the $k \sim \varepsilon$ model, using a free-slip outer boundary, plotted against the data for the radial variation of mean streamwise velocity for various axial locations. The mean velocity is normalized by the bulk mean outer velocity $\bar{U}_0 = 14.6304$ m/s (48 ft/s) and the axial location is nondimensionalized using the inner radius of the inner tube $r_0 = 9.1821$ mm (0.3615 in.). The prediction curves, though not labeled to avoid clutter, sequentially follow the data as x/r_0 increases.

As shown in Fig. 2, the inlet data for the mean velocity are quite well predicted. The acceleration of the centerline velocity is somewhat underpredicted, but not more than by about 8%. This is quite reasonable as it can be expected that experimental uncertainty may reach 15%. The radial profiles at the various locations are also underpredicted, the largest discrepancy being about 13%.

Because the data are virtually all underpredicted beyond the inlet plane, it may be surmised that the overall mass flow rate is off. The growing boundary layer at the outer radial boundary would tend to accelerate the interior fluid which could account for some of the discrepancy. To estimate this effect, the cylindrical domain is extended to a radius such that the perimeter matches that of the square experimental working section. Hence, the growing outer boundary layer causes about the same mass flow deficit as occurred in the experiment. The difference between the mass deficit caused by the

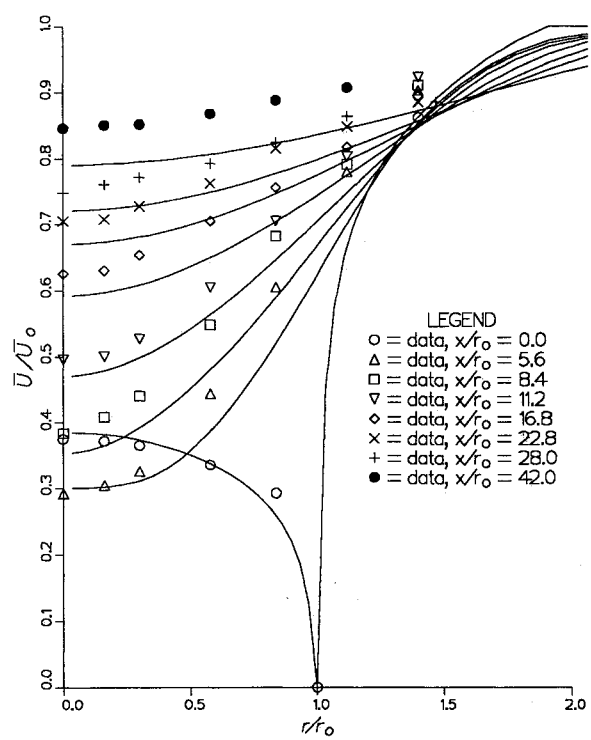

Fig. 2 Radial variation of mean axial velocity for several axial stations, constant density case; —— $k \sim \varepsilon$ results (free-slip); symbols, data of Ref. 1.

actual square apparatus in the outer developing boundary layer and the assumed circular computational domain is expected to yield at most a second-order effect, but probably a third-order effect. This effect would be the slight extra deficit caused by mutual interference of the boundary layers in the corners. A no-slip condition is used to allow the boundary-layer growth. Figure 3 illustrates results for the mixing layer while accounting for the outer boundary-layer growth. It should be noted that the radial mesh spacing has been refined by an additional 50%. The results shown in Fig. 3 indicate that some of the discrepancy of Fig. 2 is indeed the result of an acceleration of the interior flow due to a growing boundary layer. The bulk of this effect is assumed to be accounted for accurately as the outer boundary layer is predicted to grow from about 6.5 mm ($\frac{1}{4}$ in.) to about 19 mm ($\frac{3}{4}$ in.), the same values reported by Zawacki and Weinstein.[1] The maximum underprediction for Fig. 3, however, is still 15.5%. The above radial refinement of the grid as well as additional runs where the axial grid spacing was refined by a factor of three indicate that the results for the finer 66 × 81 grid are virtually grid independent.

Predictions for the thin shear ASM are given in Fig. 4. The finer grid, used for the results of Fig. 3, is used again. Inlet conditions are provided from thin shear ASM calculations of pipe and annular flows. The mean streamwise centerline velocity accelerates faster for the ASM than for the $k \sim \varepsilon$ model. However, the underprediction of the mean velocity in the developing mixing layer is somewhat greater for the ASM than for $k \sim \varepsilon$. One has to conclude that the standard $k \sim \varepsilon$ results are better than those for the ASM because the former are quantitatively closer to the data for the earlier stations (x/r_0 = 5.6, 8.4, and 11.2) (being qualitatively similar) and are qualitatively better for the outer stations. (Although the ASM results are closer to the data for $x/r_0 \geq 22.8$, they indicate a shallower $\partial\bar{U}/\partial r$ than are shown by either the data or the $k \sim e$ results.)

The behavior of the ASM can be explained in part by comparing the two forms for the turbulent shear stress, Eqs. (4) and (11). While both formulas have an explicit dependence on the factor k^2/ε, the ASM formula also contains an explicit

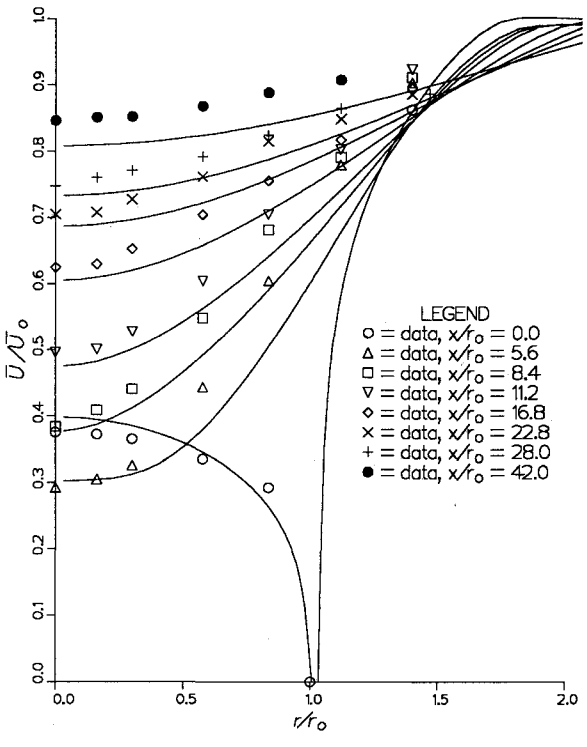

Fig. 3 Radial variation of mean axial velocity, constant density; —— $k \sim \varepsilon$ results (no-slip); symbols, data of Ref. 1.

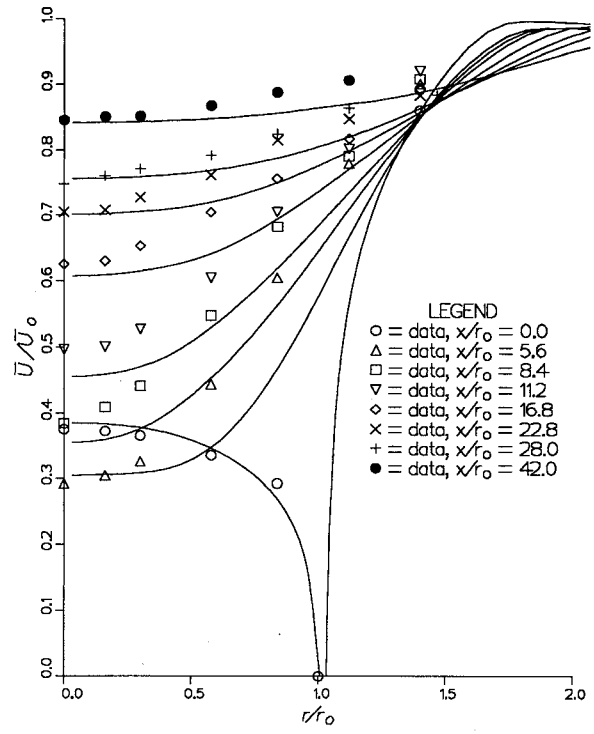

Fig. 4 Radial variation of mean axial velocity, constant density; —— ASM results (no-slip); symbols, data of Ref. 1.

dependence on the factor P/ε. When the production is high, as it is for low x/r_0, the net effect is for the "turbulent viscosity" (the coefficient of $\partial\bar{U}/\partial r$) to diminish, thereby reducing the mixing effect. For the far downstream region, however, where production of turbulent kinetic energy has decreased substantially, the net effect of the factor P/ε is to increase the viscosity, enhancing the turbulent mixing and promoting the development of the core region. Unfortunately, these effects, which are due to the nature of the ASM, are shown to be undesirable for the present flow.

Figure 5 compares predictions for the turbulent shear stress for the two models with the data for $x/r_0 \geq 8.4$. The calculations show magnitudes of roughly a factor of two greater than the data! This might lead one to conclude that the turbulent mixing rate is drastically overpredicted. However, additional computations have been made for the $k \sim \varepsilon$ model beginning at x/r_0 = 8.4 where shear stress data are reported (the same approach used by Zelazny et al.[2]). The results for the mean streamwise velocities and shear stresses are plotted in Figs. 6 and 7. While the values calculated for the shear stresses are clearly much closer to the reported data than those of Fig. 5, the results for the mean velocities are clearly poorer as the centerline velocity is more slowly accelerated than indicated for the $k \sim \varepsilon$ results (Fig. 2). Of course, the mean velocities depend on the gradients of shear stress, not its magnitude. Inspection of the shear stress predictions in Fig. 5 shows that their radial gradients are steeper than those of the data. However, we can consider the findings of other workers[4] who, as mentioned earlier, concluded that their mean data taken with a hot wire erred on the high side while their rms data were low compared to reality. (The present calculations show discrepancies vs the data in the same directions.) Furthermore, the reported discrepancies[4] of the order of 10 and 17% between LDA and hot-wire data for mean and rms data, respectively, give some indication of the experimental uncertainty. Maximum discrepancies between the data and the calculations of the mean velocity shown in Figs. 2 and 3 are 13.4 and 15.5%, respectively. A further observation is that the $k \sim \varepsilon$ model provides more than enough mixing, indicating that either countergradient diffusive transport, seen

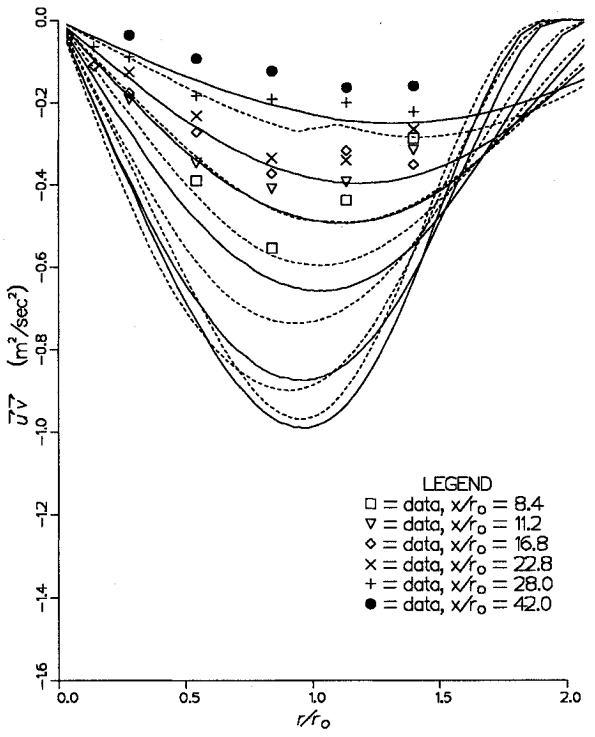

Fig. 5 Radial variation of turbulent shear stress, constant density; —— $k \sim \varepsilon$, - - - - ASM results; symbols, data of Ref. 1.

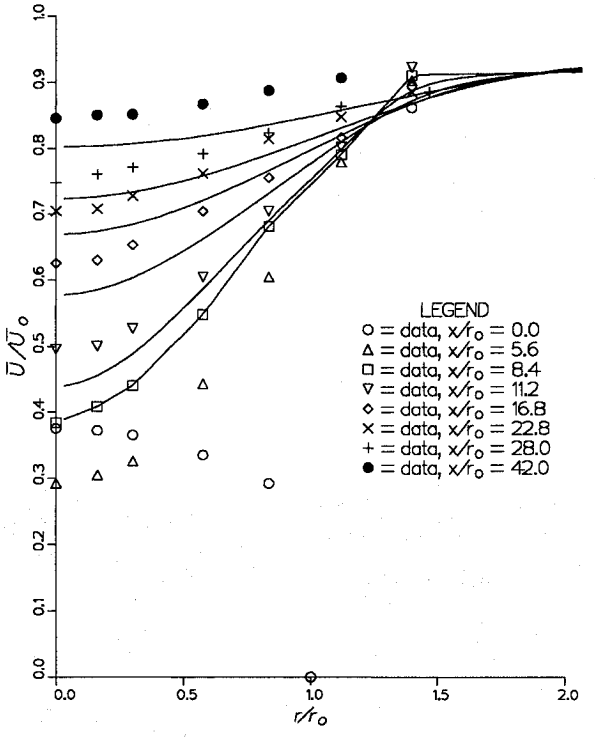

Fig. 6 Radial variation of mean axial velocity, inlet at $x/r_0 = 8.4$ (no-slip), constant density; —— $k \sim \varepsilon$; symbols, data of Ref. 1.

in related flows,[8] is small for this flow or the gradient transport provided by the model is sufficient. Indeed, it may be stated that although the $k \sim \varepsilon$ model clearly overpredicts the magnitudes of the turbulent shear stresses, though not by as much as shown in Fig. 5 given the large experimental uncertainty, and although the model may not account for countergradient diffusion, its overall performance does produce good qualitative results which are useful to the engineer, and in this case fairly close to reported data for the mean field.

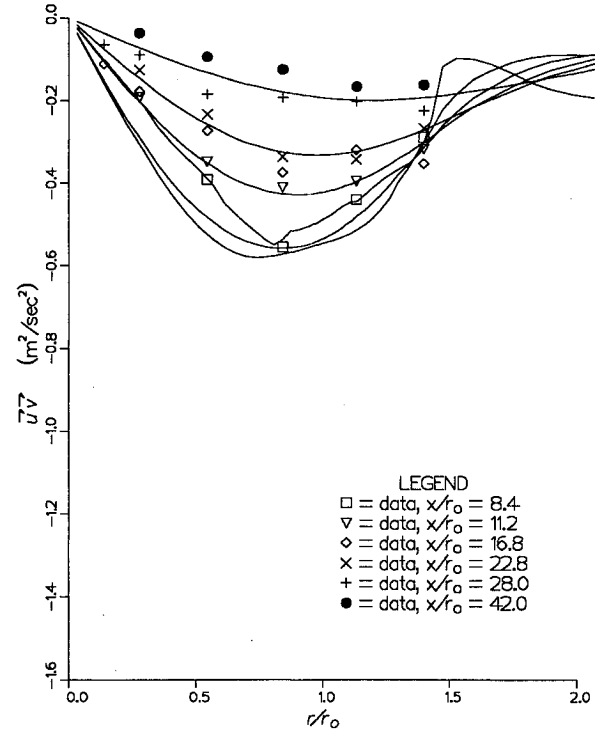

Fig. 7 Radial variation of turbulent shear stress, inlet at $x/r_0 = 8.4$ (no-slip), constant density; —— $k \sim \varepsilon$; symbols, data of Ref. 1.

In view of the above, we conclude that the $k \sim \varepsilon$ model turns in a fairly satisfactory performance for the constant density case, and proceed to extend and use it for a similar variable density flow.

Variable Density Case

Zawacki and Weinstein[1] also provide data for the case of a denser inner stream (Freon 12) flowing into an annular stream of air. They indicate that the density ratio of Freon 12 to air is $\bar{\rho}_i/\bar{\rho}_o = 4/1$, although a ratio of 4.26 to one would be computed based on properties at one atmosphere and 300 K. We use the reported 4:1 ratio. The outer to inner mean velocity ratio used for the variable density case is 3.6 as shown in Fig. 1.

Inlet plane conditions are obtained the same way as for the constant density case, except that fully developed pipe flow of Freon 12 is used for the inner stream. Figure 8 shows the results of the extended $k \sim \varepsilon$ model for the radial variation of the mean streamwise velocity for several axial stations compared with the data. The predictions, however, are for the mass-weighted mean velocity. The data were taken using a hot-wire anemometer, which is sensitive to variations in the wire Reynolds number, and hence the density, and it is not clear from the report if the data are really unweighted or effectively mass weighted. Because the agreement is as good as for the constant density case, we conclude that either the data are mass weighted or the difference is small. In either case, the results exhibit the same trend as for the constant density case; that is, the rate of mixing is overpredicted. However, we can say again that the results are fairly satisfactory for the prediction of the mean streamwise velocity.

The concentration profiles are reported in dimensionless form.[1] The local mean density is nondimensionalized according to $(\bar{\rho} - \bar{\rho}_o)/(\bar{\rho}_i - \bar{\rho}_o)$ where $\bar{\rho}_o$ is the mean density of the entering outer stream (air) and $\bar{\rho}_i$ is the mean density of the entering inner stream. Figure 9 shows the simulations for the radial variation of the dimensionless local mean density compared to the data at several axial stations. We see that the agreement is good, well within experimental uncertainty. We conclude that the extended $k \sim \varepsilon$ turbulence model per-

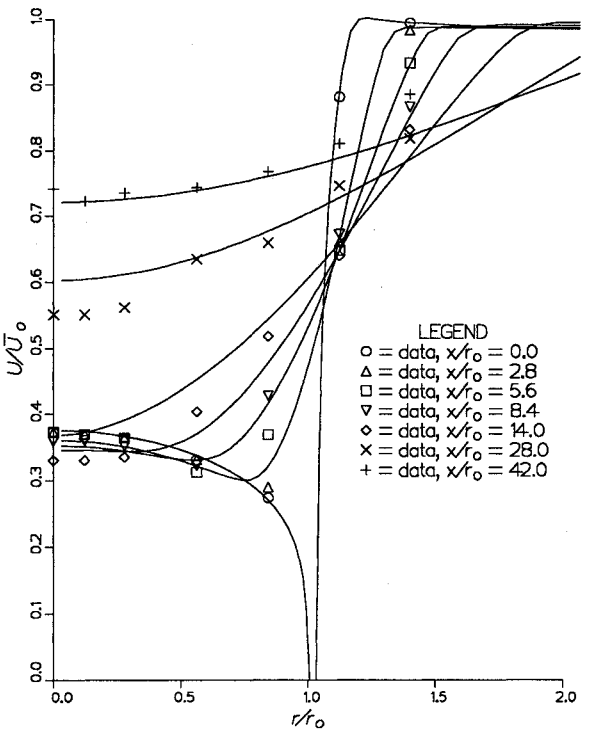

Fig. 8 Radial variation of mean axial velocity, variable density, —— extended $k \sim \varepsilon$ results (no-slip); symbols, data of Ref. 1.

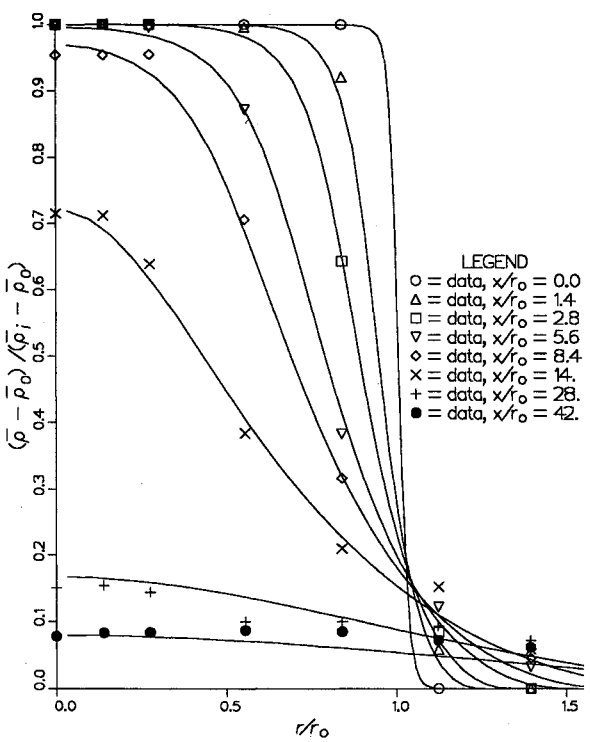

Fig. 9 Radial variation of dimensionless mean local density, —— extended $k \sim \varepsilon$ results; symbols, data of Ref. 1.

forms fairly satisfactorily for the variable density case using 0.9 for the turbulent Schmidt number and that the gradient diffusion approach of the model is suitable.

Further testing of the $k \sim \varepsilon$ model is required, however, for the mixing of fluids of much higher density ratios and at much higher temperatures to be able to assess its value for use as a modeling tool in connection with the gas core reactor. However, it would be desirable to obtain new data for the turbulent axisymmetric mixing layer, documenting completely the initial mixing plane and carefully reducing the data to obtain unambiguously either mass-weighted or unweighted velocities and the difference.

Conclusions

Numerical simulations are obtained for each of two turbulence models ($k \sim \varepsilon$ and a thin shear ASM) for incompressible, constant density, stationary, turbulent, coaxial streams and for a similar variable density flow using an extended $k \sim \varepsilon$ model. The conclusions of the present study are the following: 1) the $k \sim \varepsilon$ model velocity simulations are qualitatively satisfactory for the constant density case and for the variable density case, although excessive radial diffusion of axial momentum is predicted; 2) the thin shear ASM simulations are generally inferior to the $k \sim \varepsilon$ predictions for the constant density case; 3) the $k \sim \varepsilon$ predictions of mass transport in the variable density case show good agreement; 4) a significant portion of the errors in the predictions is likely due to inaccurate inlet conditions as the experimental inlet data are incomplete; 5) the experimental uncertainty of the data is fairly significant; 6) additional data where initial mixing plane information is completely documented are desirable; and 7) the $k \sim \varepsilon$ turbulence model appears suitable for use as a design tool for fluid machinery involving coaxial flows, at least to determine qualitative aspects of such flows.

Acknowledgments

The author wishes to acknowledge the helpful comments made by the reviewers. This work was performed at the Idaho National Engineering Laboratory, Idaho Falls, Idaho, through the EG&G Idaho Laboratory Directed Research and Development Program under DOE Field Office, Idaho, Contract DE-AC07-76ID01570.

References

[1]Zawacki, T. S., and Weinstein, H., "Experimental Investigation of Turbulence in the Mixing Region Between Coaxial Streams," NASA CR-959, Feb. 1968.

[2]Zelazny, S. W., Morgenthaler, J. H., and Herendeen, D. L., "Shear Stress and Turbulence Intensity Models for Coflowing Axisymmetric Streams," *AIAA Journal*, Vol. 11, Aug. 1973, pp. 1165–1173.

[3]Ribeiro, M. M., and Whitelaw, J. H., "Turbulent Mixing of Coaxial Jets with Particular Reference to the Near-Exit Region," *Journal of Fluids Engineering*, Vol. 98, June 1976, pp. 284–291.

[4]Habib, M. A., and Whitelaw, J. H., "Velocity Characteristics of Confined Coaxial Jets with and without Swirl," *Journal of Fluids Engineering*, Vol. 102, Mar. 1980, pp. 47–53.

[5]Ribeiro, M. M., and Whitelaw, J. H., "Coaxial Jets with and without Swirl," *Journal of Fluid Mechanics*, Vol. 96, Pt. 4, 1980, pp. 769–795.

[6]Bradshaw, P., Ferriss, D. H., and Atwell, N. P., "Calculation of Boundary-Layer Development Using the Turbulence Energy Equation," *Journal of Fluid Mechanics*, Vol. 28, 1967, p. 593.

[7]Wagner, C. A., Brondum, D. C., and Bennett, J. C., "Turbulent Navier-Stokes Computations of Confined Coaxial Jets Using a New Turbulence Model," *Proceedings of the 1st National Fluid Dynamics Congress*, AIAA/ASME/SIAM/APS, Pt. 1, 1988, pp. 592–597.

[8]Johnson, B. V., and Bennett, J. C., "Mass and Momentum Turbulent Transport Experiments with Confined Coaxial Jets," NASA CR-165574, Nov. 1981.

[9]Brondum, D. C., Bennett, J. C., Weinberg, B. C., and McDonald, H., "Numerical and Experimental Investigation of Non-swirling and Swirling Confined Jets," AIAA Paper 86-0040, Jan. 1986.

[10]Brondum, D. C., and Bennett, J. C., "Influence of Large-Scale Motion on Turbulent Transport for Confined Coaxial Jets," NASA CR-175035, Jan. 1986.

[11]Sturgess, G. J., and Syed, S. A., "Widely-Spaced Co-Axial Jet, Diffusion-Flame Combustor: Isothermal Flow Calculations Using the Two-Equation Turbulence Model," AIAA Paper 82-0113, Jan. 1982.

[12]Launder, B. E., Morse, A. P., Spalding, D. B., and Rodi, W., "Prediction of Free Shear Flows—a Comparison of the Performance of Six Turbulence Models," *Proceedings of the 1972 Langley Free Shear Flows Conference*, NASA SP321, Hampton, VA, 1973, pp.

361–425.

[13]Rodi, W., "Turbulence Modeling for Incompressible Flows," *PCH PhysicoChemical Hydrodynamics*, Vol. 7, Nos. 5 and 6, 1986, pp. 297–324.

[14]Biringen, S., "Calculation of Axisymmetric Jets and Wakes with a Three-Equation Model of Turbulence," *Journal of Fluid Mechanics*, Vol. 86, 1978, pp. 745–759.

[15]Launder, B. E., Reece, G. J., and Rodi, W., "Progress in the Development of a Reynolds-Stress Turbulence Closure," *Journal of Fluid Mechanics*, Vol. 68, 1975, pp. 537–566.

[16]Lewellen, W. S., Teske, M., and Donaldson, C. duP., "Application of Turbulence Model Equations to Axisymmetric Wakes," *AIAA Journal*, Vol. 12, No. 5, 1974, pp. 620–625.

[17]Nallasamy, M., "Computation of Confined Turbulent Coaxial Jet Flows," *Journal of Propulsion and Power*, Vol. 3, No. 3, 1987, pp. 263–268.

[18]Jones, W. P., and Launder, B. E., "The Prediction of Laminarization with a 2-Equation Model of Turbulence," *International Journal of Heat and Mass Transfer*, Vol. 15, 1972, pp. 301–314.

[19]Launder, B. E., and Spalding, D. B., "The Numerical Computation of Turbulent Flows," *Computer Methods in Applied Mechanics and Engineering*, Vol. 3, 1974, pp. 269–289.

[20]Johnson, R. W., "Turbulent Convecting Flow in a Square Duct with a 180° Bend; An Experimental and Numerical Study," Ph.D. Dissertation, Faculty of Technology, Univ. of Manchester, Manchester, England, UK, 1984.

[21]Iacovides, H., and Launder, B. E., "Turbulent Momentum and Heat Transport in Square-Sectioned Ducts Rotating in Orthogonal Mode," *Numerical Heat Transfer*, Vol. 12, 1987, pp. 475–491.

[22]Rodi, W., "The Prediction of Free Boundary Layers by Use of a 2-Equation Model of Turbulence," Ph.D. Dissertation, Faculty of Engineering, Univ. of London, London, 1972.

[23]Gibson, M. M., and Launder, B. E., "Ground Effects on Pressure Fluctuations in the Atmospheric Boundary Layer," *Journal of Fluid Mechanics*, Vol. 86, 1978, pp. 491–511.

[24]Launder, B. E., and Morse, A. P., "Numerical Prediction of Axisymmetric Free Shear Flows with a Reynolds Stress Closure," *Turbulent Shear Flows—1*, Springer-Verlag, Berlin, 1979, p. 279.

[25]Launder, B. E., "Turbulence Transport Models for Numerical Computation of Fluid Flow," Dept. of Mechanical Engineering, ME 213, Univ. of California, Davis, CA, 1980.

[26]Launder, B. E., "Heat and Mass Transport," *Topics in Applied Physics; Vol. 12—Turbulence*, edited by P. Bradshaw, Springer-Verlag, Berlin, 1976, Chap. 6, pp. 231–287.

[27]Patankar, S. V., and Spalding, D. B., "A Calculation Procedure for Heat, Mass, and Momentum Transfer in Three Dimensional Parabolic Flows," *International Journal of Heat and Mass Transfer*, Vol. 15, 1972, pp. 1787–1805.

[28]Gosman, A. D., and Ideriah, F. J. K., "TEACH-2E: A General Computer Program for Two-Dimensional Turbulent, Recirculatory Flows," Dept. of Mechanical Engineering, Imperial College, London, 1976.